C: Surfaces, Interfaces, Porous Materials, and Catalysis

DFT Study on the Effect of Aluminum Position in Zn-Exchanged MFI on Methane Activation

Sandra C Albarracín-Suazo, Yomaira J. Pagan-Torres, and Maria C. Curet-Arana

J. Phys. Chem. C, **Just Accepted Manuscript** • DOI: 10.1021/acs.jpcc.9b02487 • Publication Date (Web): 14 Jun 2019

DFT Study on the Effect of Aluminum Position in Zn-Exchanged MFI on Methane Activation

*Sandra C. Albarracín-Suazo, Yomaira J. Pagán-Torres, and María C. Curet-Arana**

Department of Chemical Engineering, University of Puerto Rico−Mayagüez Campus, Mayagüez, Puerto Rico 00681-9000, United States.

Corresponding Author

*Tel.: 787 832-4040, ext. 2569, E-mail: maria.curetarana@upr.edu

ABSTRACT

The position of aluminum atoms in ion-exchanged zeolites is known to affect the reactivity of active sites. In this work, we used DFT calculations to systematically quantify the effect of Al-atom position within the α-ring of Zn-exchanged MFI (Zn-MFI) on the activation of methane. Our DFT results indicate that the most stable configuration for the Zn-exchanged cluster of the α-ring is obtained when the Al atoms are located at the T11-T2 crystallographic sites. For each Al-atom configuration, we analyzed the reaction pathways for methane activation. Our results suggest that the activation of methane yields the formation of a Brønsted acid site, which can be formed at an oxygen atom within the α-ring or at an oxygen atom that lies outside the α-ring, and that the lowest reaction energy for methane activation is obtained when the Brønsted acid site is formed at the oxygen atom in which the HOMO of the isolated cluster is located. Furthermore, our results indicate that the partial atomic charge of the Zn atom within the α-ring of MFI can be correlated to the transition state energy of methane activation, which ranges from 87 to 131 kJ/mol depending on the location of Al atoms. The fundamental studies conducted in this work contribute to the elucidation of essential parameters and correlations, based on electrostatic and electron density, for the activation of methane on Zn-MFI zeolites.

1. INTRODUCTION

Increased methane (CH_4) availability has sparked interest in its use as a raw material to produce chemicals, such as methanol and acetic acid.[1,2] According to the U.S. Energy Information Administration (EIA), coalbed methane reserve has reached 11.8 trillion cubic feet in the United States.[3] Currently, methane is mainly used in industry for the production of syngas at temperatures higher than 973 K, which is then converted into chemicals, such as hydrocarbons or alcohols.[2] The current challenge, however, is the direct conversion of methane to value-added products due to its highly stable C-H bond, which has a dissociation energy of 438.8 kJ/mol.[2,4]

The MFI zeolite has been shown to activate methane at low temperatures when it is exchanged with zinc cations (Zn^{2+}).[5] Therefore, experimental[5–9] and theoretical[10–12] studies have focused on understanding the mechanism of hydrogen atom abstraction from methane within the pore of this zeolite. By using 1H and 13C NMR techniques, Kolyagin et al.[6] demonstrated that methane dissociates over Zn-exchanged MFI (Zn-MFI), and this dissociation yields the formation of a hydroxyl group in the zeolite, which is in agreement with other previous studies.[6,13–15] Furthermore, they found that these hydroxyl groups are stable and cause a reduction of the catalytic activity. Similarly, through in situ NMR, Stepanov et al.[16] also determined that Zn-MFI facilitates C-H bond activation in methane and ethane. They also found that the hydrogen atom is strongly attracted to an oxygen atom, thus leading to the formation of Brønsted acid sites.[13,16,17]

Different studies have been also carried out on methane activation with MFI zeolites exchanged with either oxo-clusters or metal cations, such as Cu, Fe, and Zn.[9,18–20] For the Cu-based MFI catalysts, it has been demonstrated that the oxo-clusters $[M–O–M]^{2+}$ yield lower energy barriers than metal cations. For instance, the energy barrier for methane dissociation on [Cu-O-Cu]-

exchanged MFI is 82 kJ/mol,[18] while on Cu-MFI is 129 kJ/mol.[21] However, for methane dissociation on Zn catalysts, it has been demonstrated that Zn-exchanged MFI is more active than the zinc oxides.[17]

Previous studies have aimed to analyze the Al distribution in zeolites and its possible effects in catalysis.[22,23] For instance, in an early work by Grunder and Iglesia, they concluded that the distribution of Al atoms in the T-sites of MFI can affect the energy barrier for alkane activation.[24] Subsequent studies have then confirmed this conclusion, and various studies have also reported that the Brønsted acidity of the MFI zeolite varies depending on the distribution of the aluminum atoms within the framework.[24–26] Thus, the catalyst activity can be compromised depending on this distribution, and this can yield low conversion rates. Previous studies have also aimed to pinpoint the MFI crystallographic sites in which the Al atoms are located.[15] For instance, Sklenak et al.[27] combined high resolution 27aluminum (27Al) NMR spectroscopy with density functional theory (DFT) / molecular mechanics calculations, and they established which of the 12 distinguishable T-sites of MFI zeolite are occupied by Al-atoms. Furthermore, Yokoi et al.[28] were able to control the location of Al-atoms on MFI zeolites by using different organic molecules during the synthesis of the zeolite. For instance, when tetrapropylammonium cations were used, Al-atoms are primarily located at the intersection of MFI zeolite channels.

While efforts have been put forth in studying and controlling the Al-atom distribution in various zeolites, the specific effects of this distribution on methane activation has not been thoroughly studied. Recently, Zhao et al.[29] conducted DFT studies to analyze the effect of Al positions in Cu-MOR for the oxidation of methane to methanol. They reported that methane adsorption energies ranged from 43 to 65 kJ/mol and activation energies ranged from 63 to 124 kJ/mol depending on

the position of the Al atoms within the ring. To our knowledge, a similar study on MFI zeolite, which has been more widely used for methane activation, still lacks in the literature.

In this work, we have conducted a systematic study of the effect of Al-atom location within the α-ring of Zn exchanged MFI on the energy barrier for methane activation, as described in Figure 1. Our work unravels that: (i) Al atoms distribution produces a variation in the energy barrier of methane activation, (ii) the activation of methane yields the formation of a Brønsted acid site at the oxygen in which the HOMO of the isolated cluster is located, and (iii) there is a correlation between the transition state energy of methane activation and the partial atomic charge of the Zn atom within the α-ring of MFI.

2. METHODOLOGY

Methane activation was analyzed on MFI zeolite by creating a cluster based on the crystallography data available in the Database of Zeolite Structures.[30] Here we analyzed the α-ring in MFI, which has been reported as the most active site in Zn-exchanged MFI.[31,32] Figure 1(a) shows the location of the ring within the zeolite pore. This ring is composed of seven silicon atoms, and each silicon atom corresponds to a different crystallographic T-site. The crystallographic sites are identified in Figure 1(b). In this work, the location of each Al atom within the α-ring is identified with the T-sites shown in Figure 1(b).

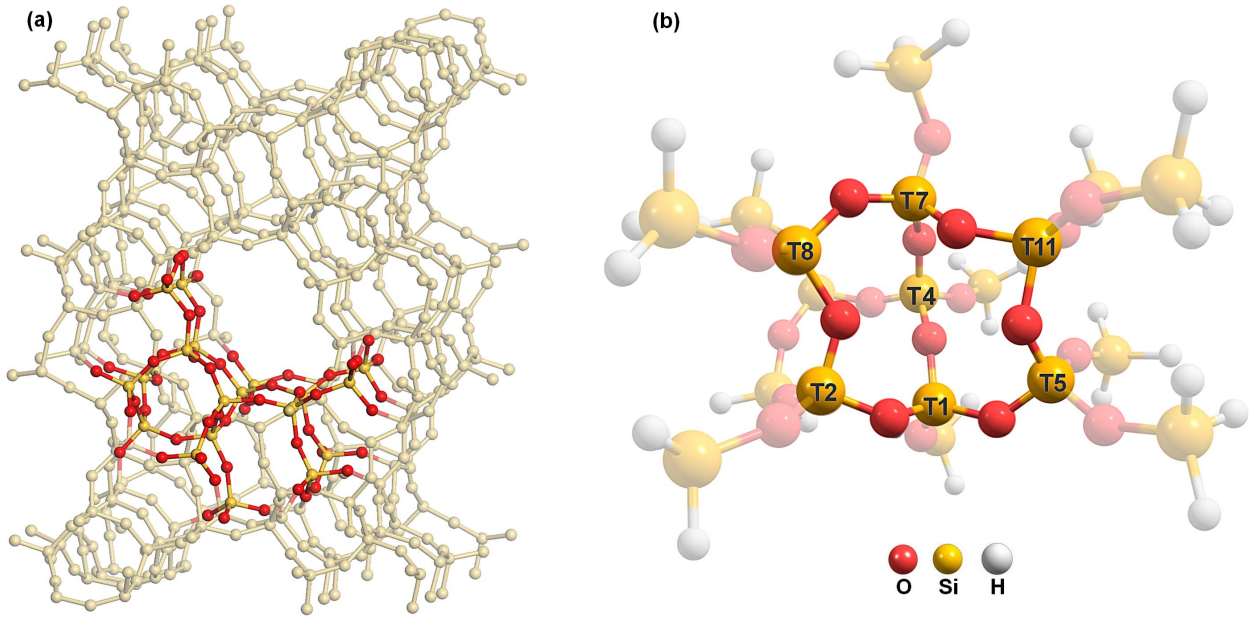

Figure 1. (a) MFI zeolite framework. The α-ring of the zeolite framework is highlighted with yellow for silicon atoms and red for oxygen atoms. **(b)** The 74-atom cluster of the α-ring of MFI used in our calculations with the corresponding crystallographic T-sites. Hydrogen atoms are shown in white.

The $ZnAl_2Si_{17}O_{22}H_{32}$ cluster analyzed in this work is composed of 74 atoms. The cluster was constructed by cutting the periodic structure, and the boundary silicon atoms were saturated with hydrogen atoms. These hydrogen atoms were aligned along the same direction of the oxygen atoms that were removed, and the Si−H bond lengths were set to 1.50 Å. Two Al atoms were substituted within the α-ring to stabilize the Zn^{2+} charge on the cluster.[33] As illustrated in Figure 1(b), the α-ring of MFI has seven silicon atoms. We systematically analyzed the clusters that can be formed by replacing two Si atoms within the α-ring with two Al atoms. We further performed geometry optimizations on the clusters, and no symmetry constraints was imposed in any of the systems. Thus, we considered all the different configurations in which the Al atoms could be located within the α-ring. The only constraint that we followed was the Loewenstein rule, which specifies that there cannot be two consecutive AlO_4 tetrahedra.[34] Therefore, clusters containing Al-O-Al sequences were not considered in this work. As shown in Figure 2(b), this results in 13 different

configurations. All geometrical optimizations were performed on neutral charge clusters with singlet spin state.

All calculations conducted in this work used ωB97XD as the exchange-correlation functional, which is a long-range corrected functional.[32] The basis set LANL2DZ[35] was used for the Zn atom, while 6-31+g**[36] was used for Al, O, Si, H, and, C atoms. In all geometry optimization calculations, all atoms within the cluster were relaxed, except for the terminal H-atoms that were kept fixed. The methodology that we employed in this work has been previously applied and validated by different authors for the computational study of zeolites, such as MFI,[37,38] BEA,[39,40] and FAU.[41,42] The partial atomic charges were obtained with the natural bond orbital (NBO) population analysis.[43] Vibrational frequencies were calculated for each optimized structure, within the rigid-rotor, harmonic-oscillator approximation. All the transition states were corroborated by displaying only one imaginary frequency along the reaction coordinate. All calculations were performed with Gaussian 09.[44]

3. RESULTS AND DISCUSSION

The relative energies of the MFI α-ring isolated clusters with respect to the most stable Al atom configuration are compared in Figure 2(a). The **T11-T2** structure is the most stable configuration, followed by **T11-T1**. The most unstable cluster is **T5-T4**, and it is 113 kJ/mol higher in energy than **T11-T2**. By comparing some of the geometrical parameters among the optimized α-ring clusters, we note that the Zn atom is always located at the center of the α-ring, and it is coordinated to four oxygen atoms in all configurations. On the isolated clusters, the Zn atom has a square planar arrangement with respect to the oxygen atoms on the α-ring. Our calculated Zn-O distances in the isolated clusters are comparable to the Fe-O distances reported on Fe-exchanged MFI. The

differences on the bond lengths range from 0.7 % when Al-atoms are located on the T7-T1 sites up to 2.2 % on the T11-T2 Al-configuration.[45] Similarly, the Zn-O distances are also comparable to those reported by Montejo-Valencia et al. on Cu-exchanged MFI.[21] The reported Cu-O bond lengths are just 3.4% lower than those that we obtained for Zn-O. The Al-Zn distances in each cluster, which range from 2.75 to 3.36 Å, are reported in Table S1 in the Supporting Information. We note that in **T11-T2**, which is the lowest energy configuration, the two Zn-Al distances are equal, with a value of 2.91 Å. We also note that the O-Al-O angles formed on that configuration are very similar, with values of 89.2° in T11, and 91.0° in T2 site. Thus, the inclusion of the Al atoms at **T11** and **T2** crystallographic sites yields a quasi-symmetric structure with similar distances and angles, in contrast to the other configurations, in which the angles and distance parameters are not symmetric.

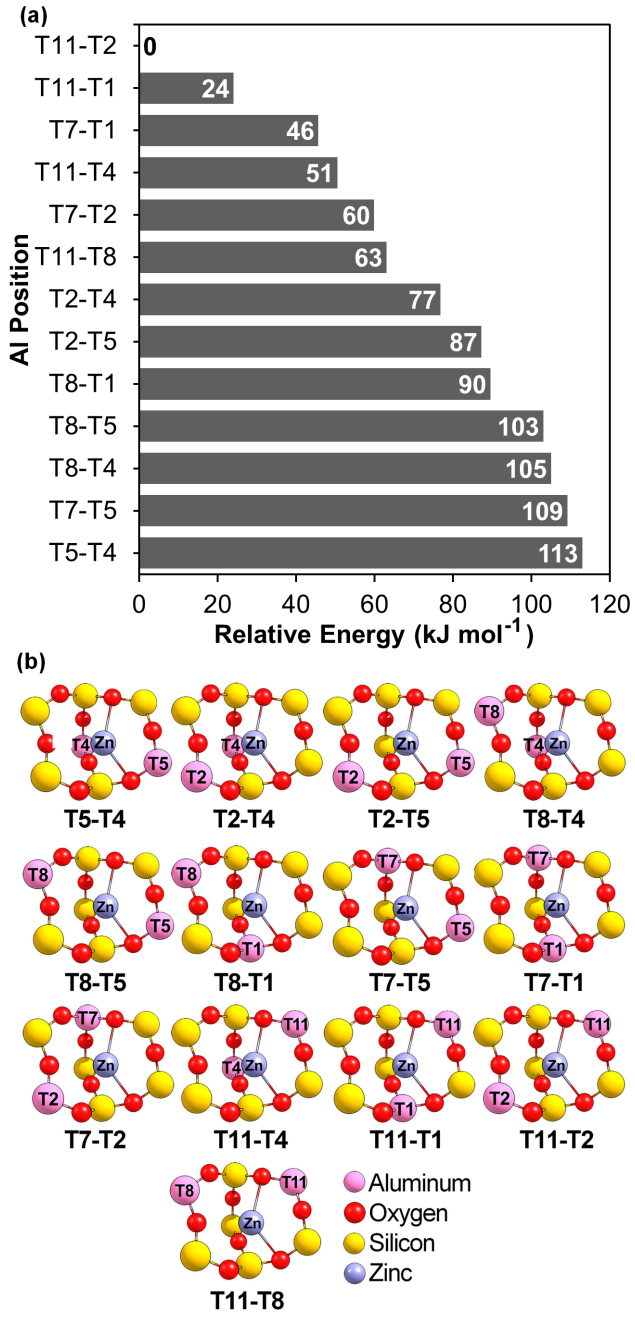

Figure 2. (a) Relative energy of the MFI α-ring cluster with respect to the lowest energy configuration, T11-T2. **(b)** Schematic representation of the 13 Al configurations of the α-ring. Atoms beyond the α-ring were removed from the figures for clarity.

Methane activation involves two elementary steps: (1) methane adsorption and (2) detachment of a hydrogen atom to form methyl (CH3) and an –OH Brønsted site. The –OH Brønsted site can be formed in any of the oxygen atoms within the α-ring or in an oxygen atom adjacent to the α-ring. It is known that the location of the –OH Brønsted site yields different reaction energies in methane activation.[21] Hence, we have systematically analyzed two plausible reaction paths for methane activation on all the 13 Al-atom configurations of the α-ring of Zn-MFI, depending on whether the Brønsted site is formed on an external oxygen atom, **Oe**, or an internal oxygen atom, **Oi**. For example, Figure 3 shows the location of the oxygen atoms in which the –OH Brønsted sites can be formed on the **T11-T2** Al configuration. In that figure, we labeled the oxygen atoms within the α-ring as **Oi-*n*,** where *n* is a number from one to four, and the external oxygen atoms that are located outside the α-ring as **Oe-*n***.

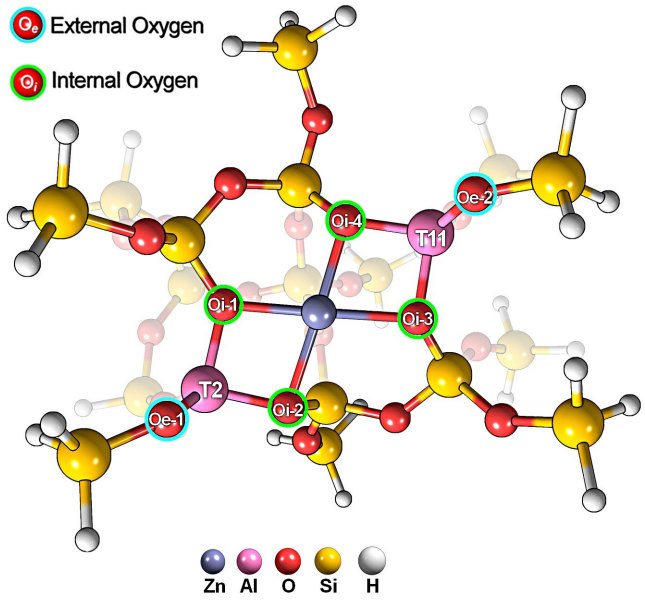

Figure 3. Oxygen atoms in which the –OH Brønsted acid can be formed in the **T11-T2** configuration. **Oe**, highlighted in light blue, denotes the oxygen atoms located outside the α-ring. **Oi**, highlighted in light green, denotes the oxygen atoms within the α-ring.

Once the internal and external oxygen atoms were identified, we analyzed the minimum energy path. For each of the 13 Al configurations shown in Figure 2(b), we calculated the reaction energies for methane dissociation, by considering all possible oxygen atoms in which the -OH Brønsted site can be formed on each cluster. In this work, we considered the formation of hydroxyl groups on the oxygen atoms that are directly bonded to the Al atoms. Thus, the total number of Brønsted sites that can be formed varies depending on the Al configuration. For instance, Figure 4 shows the reaction energies when the Al atoms are located on the **T8-T5** crystallographic sites. For this configuration, the reaction energies for methane dissociation range from 5 kJ/mol up to 93 kJ/mol. All the reaction energies obtained for H abstraction are endothermic. The reaction energies for the 13 Al atom configurations shown in Figure 2(b) are tabulated in Figure S2 in the Supporting Information.

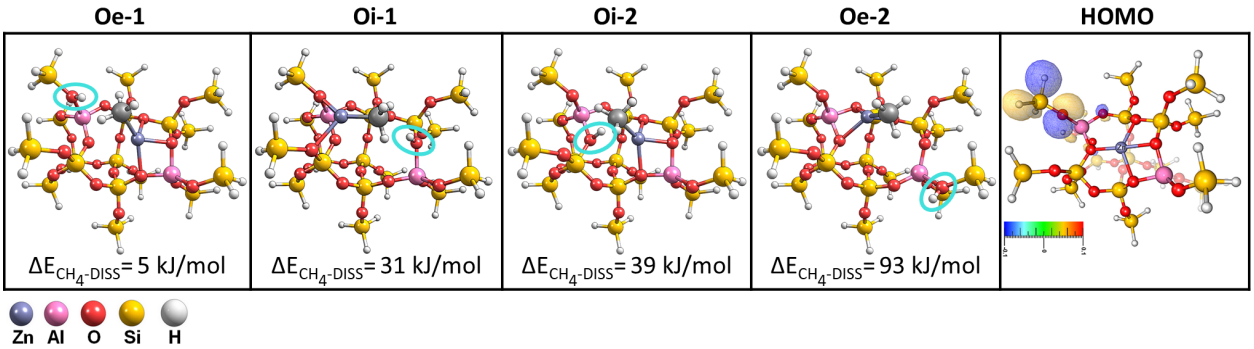

Figure 4. Reaction intermediates that can be formed upon methane activation with the various oxygen atoms on the α-ring of Zn-MFI when Al atoms are in **T8-T5** crystallographic sites, and the HOMO of the isolated Zn-MFI cluster. Reaction energies for the formation of the intermediates were calculated with the energy of the isolated species as reference, i.e. $\Delta E_{CH4\text{-}DISS} = E_{complex} - (E_{methane} + E_{Zn\text{-}MFI\text{-}T8\text{-}T5})$.

In Figure 4, we also illustrate the highest occupied molecular orbital (HOMO) for the isolated cluster when the Al atoms are located on the crystallographic sites **T8-T5**. Our results indicate that for a specific Al configuration, the lowest reaction energy for methane dissociation is obtained when the Brønsted acid site is formed on the oxygen atom in which the HOMO of the isolated

cluster is located. For the configuration shown in Figure 4, the lowest reaction energy was obtained when the Brønsted site is formed on **Oe-1**. Figure S3 in the Supporting Information illustrates the HOMO's for each isolated cluster along with all the reaction energies. Based on these results, the location of the HOMO orbital can be used to identify the oxygen atom in which the formation of the Brønsted site would yield the lowest reaction energy for methane dissociation.

We analyzed two plausible reaction paths for methane dissociation on each of the clusters on the α-ring configurations of Zn-MFI, as shown in Scheme 1. Complex **I** corresponds to the isolated species, i.e. methane and the cluster of the Zn-MFI zeolite. The first step in the reaction mechanism is methane adsorption to form Complex **II**, in which methane is physisorbed on the zeolite. The carbon atom of methane is attracted to the positive charge of the Zn atom, but no chemical bond is formed. For all the Al configurations that were analyzed, methane physisorption is exothermic with minimal variations among adsorption energies. The values of these energies range between -36 to -48 kJ/mol corresponding to **T7-T5** and **T8-T5**, respectively. Our calculations demonstrate that upon methane physisorption, the geometrical parameters of the α-ring in Complex **II** are nearly identical to the isolated counterparts. More pronounced differences, however, are obtained when comparing the distances between the zinc and carbon atom in Complex **II** on the different Al configurations. These distances vary from 2.49 to 2.70 Å, as shown in Table S2 in the Supporting Information.

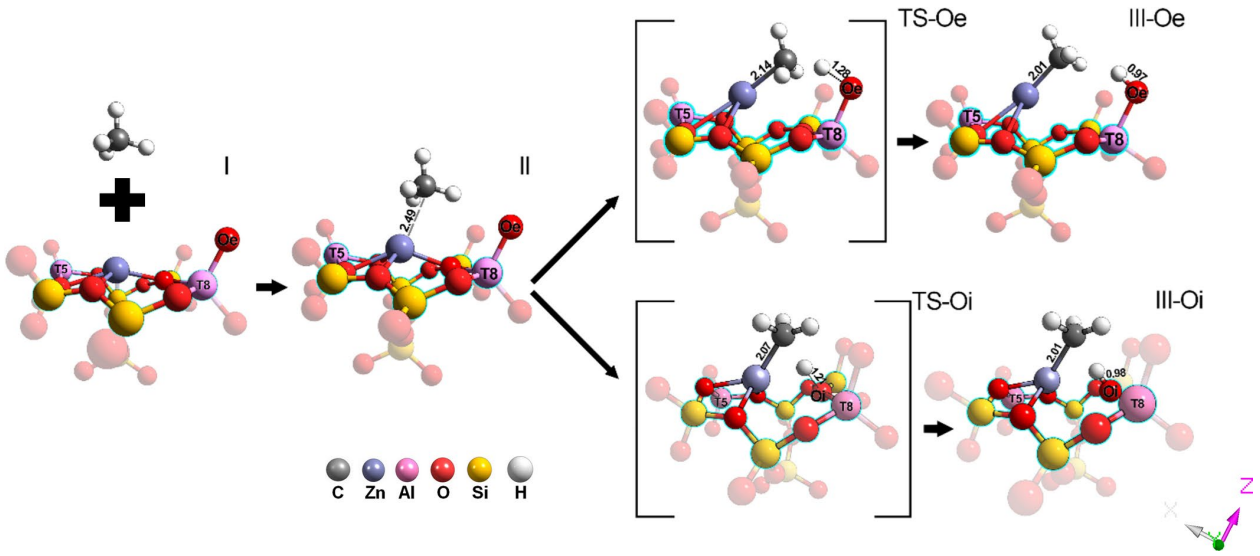

Scheme 1. Reaction mechanisms studied for methane activation on Zn-MFI α-ring for the clusters in which the Al atoms are located on **T8-T5** crystallographic sites. The most energetically favorable path involves the formation of the Brønsted acid in an external oxygen atom of the α-ring. Atoms beyond the α-ring were removed from the figures for clarity.

In complex **III-Oe**, the Brønsted site is formed with an external oxygen atom (**Oe**), whereas in complex **III-Oi** the Brønsted site is formed inside the α-ring, with an internal oxygen atom (**Oi**) as depicted in Scheme 1. The energies of these two complexes are different. The energies, relative to the isolated species in complex **I**, are 5 kJ/mol for complex **III-Oe** and 39 kJ/mol for complex **III-Oi**. The transition states to form complexes **III-Oe** and **III-Oi** (i.e., **TS-Oe** and **TS-Oi**, respectively) are also different. The energy of **TS-Oe** is 87 kJ/mol, while the energy of **TS-Oi** is 121 kJ/mol. Thus, when the Al atoms are located on the **T8-T5** crystallographic sites, the minimum energy path for methane activation is through the formation of a -OH Brønsted acid site on an external oxygen atom. Figure 5 shows the minimum energy reaction pathways for the 13 Al configurations of the α-ring of Zn-MFI. Figure 5(a) illustrates the results for the systems in which the minimum energy path for methane activation occurs through an external oxygen atom of the α-ring. Figure 5(b) illustrates the results of the systems in which methane activation is more

favorable to occur through an internal oxygen atom within the α-ring. We included in Table S3 in the Supporting Information the energy barriers, which take into account the energy of methane adsorption.

Our calculations demonstrate that the geometrical parameters of the α-ring of the clusters in complex **III** are modified upon methane activation. For instance, the distance between C and Zn atoms is decreased in all Al-arrays, resulting in the bond formation between these two atoms. For all the Al configurations, the Zn-C bond length was on average 2.01Å, suggesting that the Zn-C distance is independent of the location of the Brønsted site. This bond length is in good agreement with the experimental value reported by Haaland et al.,[46] with an error of 2.5%. The formation of the Zn-C bond causes the Zn atom to lose a coordination with one of the oxygen atoms within the α-ring, and this is reflected through the increase of the Zn-O distance. For instance, in the **T8-T5** Al-configuration the Zn-O distance increased from 2.11 to 3.03 Å. The Zn-O distances for the isolated clusters, for the transition states, and for complex **III** are tabulated in Tables S4, S5 and S6 in the Supporting Information.

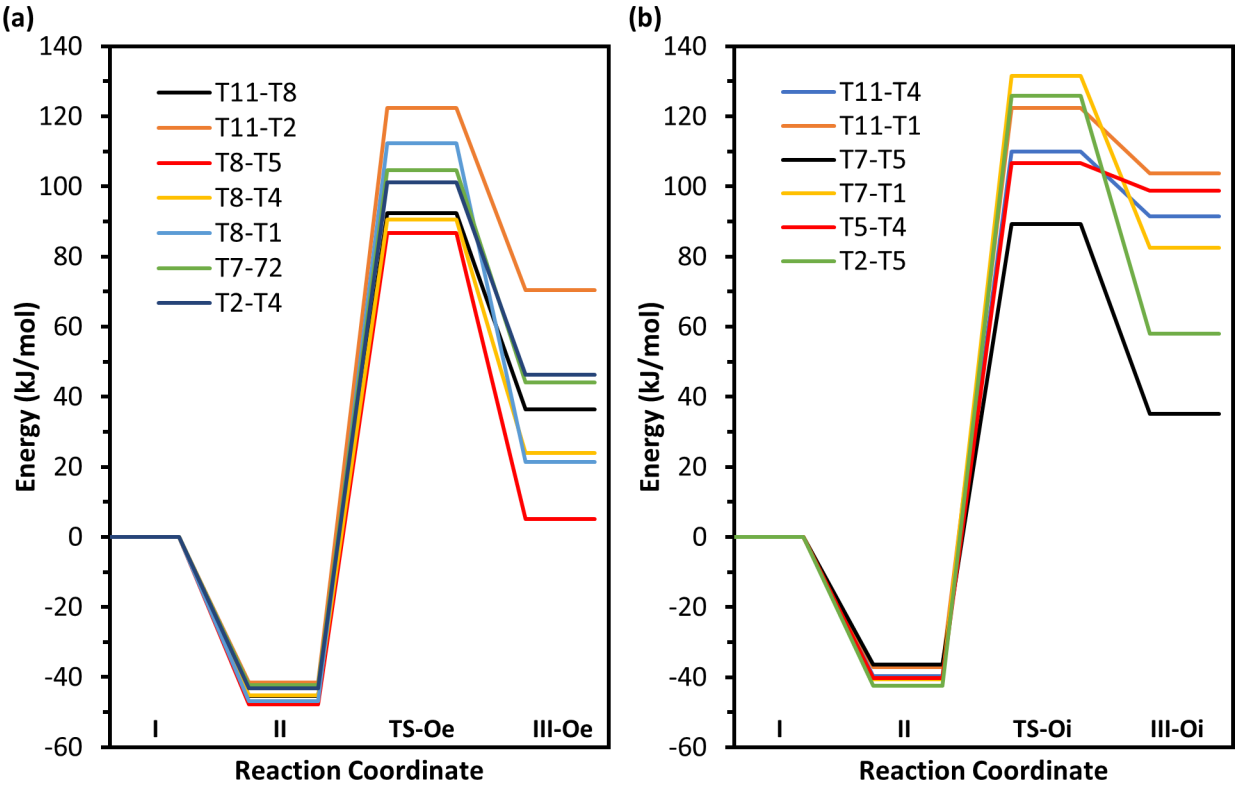

Figure 5. Minimum energy path for methane activation on the a-ring of Zn-MFI for all the Al configurations illustrated in Figure 2(b). For each Al configuration, the zero energy corresponds to the isolated cluster and methane. Complexes I, II, III, TS-Oe and TS-Oi are identified in Scheme 1. **(a)** Energy diagrams for the systems in which the hydrogen abstraction occurs through an external oxygen atom, **Oe**, and **(b)** through an internal oxygen atom, **Oi**, of the α-ring.

As shown in Figure 5(a) and (b), the energies barriers to form the transition states **TS-Oe** and **TS-Oi** vary significantly depending on the Al atom configuration on the α-ring. TS energies to form **TS-Oe** range from 87 to 122 kJ/mol, and TS energies to form **TS-Oi** range from 89 to 131 kJ/mol. We note that the most stable Al configuration of the isolated cluster, **T11-T2**, yields an activation barrier of 122 kJ/mol, which is the highest barrier obtained. In contrast, the lowest barrier to form **TS-Oi** was 89 kJ/mol on **T7-T5**, whereas the lowest barrier to form **TS-Oe** was 87 kJ/mol on **T8-T5**. The energy barriers that we have obtained are in good agreement with the energy barrier reported in the literature of 96 kJ/mol.[21] Nevertheless, we note that the energy barriers that

we calculated differ to those reported by Arzumanov et al.[7] The discrepancy in the energies is probably due to the differences in the material. Arzumanov et al. reported that the Brønsted acid sites in the zeolite could act as cocatalysts by weakening the C-H bond in methane. In this work, however, we calculated the energy barriers on a catalyst that has no Brønsted acid sites prior to the reaction. Future work should address the impact of the Brønsted acid sites on the kinetics of methane activation.

We also note that the energy barriers that we obtained are comparable to the energy barrier that has been reported for methane dissociation on Cu-exchanged MFI with the same Al-atoms configuration, with a difference of only 10 kJ/mol.[21] On the other hand, the energy barriers on Zn-MFI are significantly lower than the energy barrier reported for Fe-MFI of 169 kJ/mol when oxo-clusters [Fe–O–Fe] are the active site.[20]

In all transition states geometries, the Zn-C distance decreases when compared to those obtained in complex **II**, and it ranges from 2.07 to 2.21 Å. Furthermore, we note that transition state structures involving an external oxygen atom yield higher deformations in the zeolite than **TS-Oi.** For instance, when an external oxygen atom is involved in the transition state there is an increase of up to 16 % in the O-Al-O angle on **TS-Oe** when compared to the angle on complex **II**. On the other hand, on **TS-Oi** the maximum increase in that angle is 7 %. As shown in Figure 5(a) and (b), the overall reaction energies for the formation of complexes **III-Oe** and **III-Oi** are different for each Al configuration. Reaction energies range from 5 kJ/mol to 70 kJ/mol when an external oxygen atom is involved, and from 35 kJ/mol to 104 kJ/mol when an internal oxygen atom participates in the reaction. The **T8-T5** structure yields the lowest reaction energy for methane activation, with an overall reaction energy of 5 kJ/mol.

The acidity of the zeolites has been widely suggested to affect its catalytic activity.[47–49] While a debate still exists on how to accurately measure zeolite acidity, previous works have related the energy of the lowest occupied molecular orbital (E_{LUMO}) to the Lewis acidity of zeolites.[50] In order to verify if E_{LUMO} can be correlated to the catalytic activity of the zeolite, we plotted the TS energies with the corresponding LUMO energy of the isolated clusters as shown in Figure S4 in the Supporting Information. Our calculations demonstrate that the LUMO energies are not appropriate descriptors of the TS energies for this particular system, since no clear trend is obtained in the two reaction pathways analyzed in this work. However, we note that the lowest LUMO energy corresponds to the **T8-T5** Al configuration, which is the configuration with the lowest TS energy.

The Al-atom distribution within the active site of Zn-MFI can significantly affect the energy required for the abstraction of the H atom of methane. Thus, we further analyzed the effect of the Al position on the active site of Zn-MFI, and our calculations demonstrate that the partial atomic charge of the Zn atom ($\boldsymbol{q}_{\mathbf{Zn}}$) varies depending on the position of the Al atoms within the α-ring of MFI. The partial atomic charge $\boldsymbol{q}_{\mathbf{Zn}}$ ranged from 1.57 for **T5-T4** to 1.63 for **T8-T5**. All the values are shown in Table S1 in the Supporting Information. Our calculations further revealed that these partial charges, $\boldsymbol{q}_{\mathbf{Zn}}$**,** could be correlated to the energy barrier of methane dissociation. Figure 6(a) shows the trends for the Al configurations in which the minimum energy path leads to the formation of complex **TS-Oi**. For the clusters in which it is energetically more favorable to form the Brønsted site within the α-ring of Zn-MFI, the energy of the transition state decreases as the charge of the Zn atom decreases. However, for the clusters in which it is favorable to form the Brønsted site outside the α-ring, the transition state energy decreases with increasing charge of the Zn atom, as shown in Figure 6(b). Trends are also maintained with enthalpies and Gibbs free

energies, as shown in Figure S5 in the Supporting Information. The location of the Al-atoms has an impact on the electronic density along the α-ring, which is manifested through the partial atomic charges and the electrostatic potential of the isolated clusters. The NBO charges and the electrostatic potentials of the 13 isolated clusters are illustrated in Table S7 in the Supporting Information. We note that the different electrostatic environments directly affect the strength through which the Zn and the C atoms interact, and also this impacts the geometry of the transition state. For instance, Zn-C distance in the methane physisorption in complex **II** varies depending on the partial atomic charge of the Zn atom. Furthermore, the distance between the H-atom and the oxygen that is involved in the transition state also varies depending partial atomic charge of the Zn atom. Thus, the Al atom position within the active site of Zn-MFI affects the partial atomic charge of the Zn atom, which also impacts the energy barrier in these catalytic systems. Therefore, these results suggest that the Al-atom position could be a design parameter that could be optimized to improve the catalysis of methane activation.

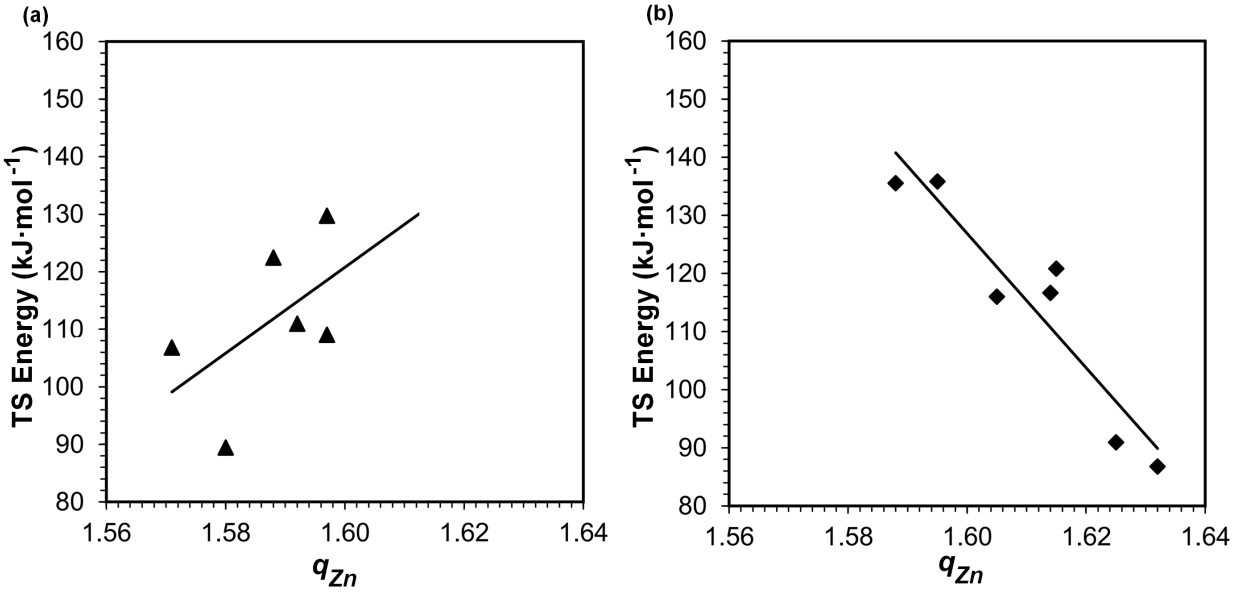

Figure 6. Transition state energies relative to the isolated species as function of the partial atomic charge of the Zn atom in the isolated cluster (I). **(a)** Transition state energies for H-atom abstraction

through an **Oi** atom in the α-ring (▲) and **(b)** transition state energies for H-atom abstraction through an **Oe** atom in the α-ring (♦).

4. CONCLUSIONS

We have conducted a systematic DFT study to analyze the effect of Al atom distribution within the α-ring of Zn-MFI on the activation of methane. We analyzed 13 different clusters of the α-ring of Zn-MFI. Our results demonstrate that the most stable configuration for the Zn-exchange cluster of the α-ring is obtained when the Al atoms are at the **T11-T2** crystallographic sites. Our results indicate that physisorption energies of methane on the active site of the Zn-exchanged MFI cluster are independent of the configuration of Al atoms in the α-ring, with physisorption energies that range from -36 to -48 kJ/mol. The activation of methane takes place on Zn, and upon activation a hydrogen atom binds to an oxygen atom of the zeolite framework. This reaction yields the formation of a Brønsted –OH acid site, which can be formed at an oxygen atom within the α-ring or at an oxygen atom that lies outside the α-ring. For each of the 13 clusters, we analyzed the reaction pathways with all the possible oxygen atoms. Our calculations revealed that for all the Al-configurations, the lowest reaction energies were obtained when the Brønsted -OH site is formed at the oxygen atom in which the HOMO of the isolated cluster is located. Furthermore, our results revealed that the Al-atom configurations affects the partial atomic charge of the Zn-atom, and this partial charge can be correlated to the transition state energy of methane activation. The fundamental studies conducted in this work aims to provide a correlation based on the electron density for the activation of methane on Zn-MFI zeolites. This work contributes to the rational design of catalytic materials for methane activation, which can provide experimentalist with insights on the synthesis of highly active zeolite catalyst for methane activation.

Supporting Information

Geometric parameters of the configurations on the reaction mechanism, reaction energies for methane activation, and HOMOs and LUMOs of each isolated Zn-MFI cluster (PDF) xyz coordinates of stable intermediates and transition states (ZIP)

Notes

The authors declare no competing financial interests.

ACKNOWLEDGMENTS

This work was supported by the National Science Foundation under Award No. 1827894 and Award No. OIA-1632824. This research used computational resources of the National Energy Research Scientific Computing Center, which is supported by the Office of Science of the U.S. Department of Energy under Contract No. DE-AC02-05CH11231, and the High-Performance Computing Facility of the Institute for Functional Nanomaterials supported by NSF through Award No. EPS-1002410 and Award No. EPS-1010094.

REFERENCES

(1) Narsimhan, K.; Iyoki, K.; Dinh, K.; Román-Leshkov, Y. Catalytic Oxidation of Methane into Methanol over Copper-Exchanged Zeolites with Oxygen at Low Temperature. *ACS Cent. Sci.* **2016**, *2* (6), 424–429.

(2) Wang, B.; Albarracín-Suazo, S.; Pagán-Torres, Y.; Nikolla, E. Advances in Methane Conversion Processes. *Catal. Today* **2017**, *285*, 147–158.

(3) U.S. Energy Information Administration. Coal-Bed Methane: Reserves https://www.eia.gov/dnav/ng/ng_enr_coalbed_dcu_NUS_a.htm (accessed on Jun 14, 2019).

(4) Hammond, C.; Conrad, S.; Hermans, I. Oxidative Methane Upgrading. *ChemSusChem* **2012**, *5* (9), 1668–1686.

(5) Gabrienko, A. A.; Arzumanov, S. S.; Luzgin, M. V; Stepanov, A. G.; Parmon, V. N. Methane Activation on Zn^{2+}-Exchanged ZSM-5 Zeolites. The Effect of Molecular Oxygen Addition. *J. Phys. Chem. C* **2015**, *119* (44), 24910–24918.

(6) Kolyagin, Y. G.; Ivanova, I. I.; Pirogov, Y. A. 1H and 13C MAS NMR Studies of Light Alkanes Activation over MFI Zeolite Modified by Zn Vapour. *Solid State Nucl. Magn. Reson.* **2009**, *35* (2), 104–112.

(7) Arzumanov, S. S.; Gabrienko, A.; Freude, D.; Stepanov, A. G.; Sun, X.; Zhou, S.;

Schlangen, M.; Schwarz, H. Competitive Pathways of Methane Activation on Zn^{2+}-Modified ZSM-5 Zeolite: H/D Hydrogen Exchange with Brønsted Acid Sites versus Dissociative Adsorption to Form Zn-Methyl Species. *Chem. - A Eur. J.* **2016**, *6*, 1–8.

(8) Kolyagin, Y. G.; Ivanova, I. I.; Ordomsky, V. V.; Gedeon, A.; Pirogov, Y. A. Methane Activation over Zn-Modified MFI Zeolite: NMR Evidence for Zn-Methyl Surface Species Formation. *J. Phys. Chem. C* **2008**, *112* (50), 20065–20069.

(9) Xu, J.; Zheng, A.; Wang, X.; Qi, G.; Su, J.; Du, J.; Gan, Z.; Wu, J.; Wang, W.; Deng, F. Room Temperature Activation of Methane over Zn Modified H-ZSM-5 Zeolites: Insight from Solid-State NMR and Theoretical Calculations. *Chem. Sci.* **2012**, *3* (10), 2932–2940.

(10) Blaszkowski, S. R.; Nascimento, M. A. C.; van Santen, R. A. Activation of C−H and C−C Bonds by an Acidic Zeolite: A Density Functional Study. *J. Phys. Chem.* **1996**, *100* (9), 3463–3472.

(11) Oda, A.; Torigoe, H.; Itadani, A.; Ohkubo, T.; Yumura, T.; Kobayashi, H.; Kuroda, Y. Mechanism of CH_4 Activation on a Monomeric Zn^{2+}-Ion Exchanged in MFI-Type Zeolite with a Specific Al Arrangement: Similarity to the Activation Site for H2. *J. Phys. Chem. C* **2013**, *117* (38), 19525–19534.

(12) Pidko, E. A.; Van Santen, R. A. Activation of Light Alkanes over Zinc Species Stabilized in ZSM-5 Zeolite: A Comprehensive DFT Study. *J. Phys. Chem. C* **2007**, *111* (6), 2643–2655.

(13) Bhan, A.; Iglesia, E. A Link between Reactivity and Local Structure in Acid Catalysis on Zeolites. *Acc. Chem. Res.* **2008**, *41* (4), 559–567.

(14) Zhu, X.; Liu, S.; Song, Y.; Xu, L. Catalytic Cracking of C4 Alkenes to Propene and Ethene: Influences of Zeolites Pore Structures and Si/Al_2 Ratios. *Appl. Catal. A Gen.* **2005**, *288* (1), 134–142.

(15) Katada, N.; Suzuki, K.; Noda, T.; Sastre, G.; Niwa, M. Correlation between Brønsted Acid Strength and Local Structure in Zeolites. *J. Phys. Chem. C* **2009**, *113* (44), 19208–19217.

(16) Stepanov, A. G.; Arzumanov, S. S.; Gabrienko, A. A.; Parmon, V. N.; Ivanova, I. I.; Freude, D. Significant Influence of Zn on Activation of the C-H Bonds of Small Alkanes by Brønsted Acid Sites of Zeolite. *ChemPhysChem* **2008**, *9* (17), 2559–2563.

(17) Gabrienko, A. A.; Arzumanov, S. S.; Toktarev, A. V; Danilova, I. G.; Prosvirin, I. P.; Kriventsov, V. V; Zaikovskii, V. I.; Freude, D.; Stepanov, A. G. Different Efficiency of Zn^{2+} and ZnO Species for Methane Activation on Zn-Modified Zeolite. *ACS Catal.* **2017**, *7* (3), 1818–1830.

(18) Arvidsson, A. A.; Zhdanov, V. P.; Carlsson, P.-A.; Grönbeck, H.; Hellman, A. Metal Dimer Sites in ZSM-5 Zeolite for Methane-to-Methanol Conversion from First-Principles Kinetic Modelling: Is the $[Cu–O–Cu]^{2+}$ Motif Relevant for Ni, Co, Fe, Ag, and Au? *Catal. Sci. Technol.* **2017**, *7* (7), 1470–1477.

(19) Arzumanov, S. S.; Gabrienko, A. A.; Freude, D.; Stepanov, A. G. Competitive Pathways of Methane Activation on Zn^{2+}-Modified ZSM-5 Zeolite: H/D Hydrogen Exchange with Bronsted Acid Sites versus Dissociative Adsorption to Form Zn-Methyl Species. *Catal. Sci. Technol.* **2016**, *6* (16), 6381–6388.

(20) He, M.; Zhang, J.; Sun, X.-L.; Chen, B.-H.; Wang, Y.-G. Theoretical Study on Methane Oxidation Catalyzed by Fe/ZSM-5: The Significant Role of Water on Binuclear Iron Active Sites. *J. Phys. Chem. C* **2016**, *120* (48), 27422–27429.

(21) Montejo-Valencia, B. D.; Pagán-Torres, Y. J.; Martínez-Iñesta, M. M.; Curet-Arana, M. C. Density Functional Theory (DFT) Study To Unravel the Catalytic Properties of M-

Exchanged MFI, (M = Be, Co, Cu, Mg, Mn, Zn) for the Conversion of Methane and Carbon Dioxide to Acetic Acid. *ACS Catal.* **2017**, *7* (10), 6719–6728.

(22) Frisch, M. J.; Pople, J. A.; Binkley, J. S. Self-consistent Molecular Orbital Methods 25. Supplementary Functions for Gaussian Basis Sets. *J. Chem. Phys.* **1984**, *80* (7), 3265–3269.

(23) Beagley, B.; Dwyer, J.; Fitch, F. R.; Mann, R.; Walters, J. Aluminum Distribution and Properties of Faujasites. Basis of Models and Zeolite Acidity. *J. Phys. Chem.* **1984**, *88* (9), 1744–1751.

(24) Gounder, R.; Iglesia, E. Catalytic Consequences of Spatial Constraints and Acid Site Location for Monomolecular Alkane Activation on Zeolites. *J. Am. Chem. Soc.* **2009**, *131* (5), 1958–1971.

(25) Sazama, P.; Dědeček, J.; Gábová, V.; Wichterlová, B.; Spoto, G.; Bordiga, S. Effect of Aluminium Distribution in the Framework of ZSM-5 on Hydrocarbon Transformation. Cracking of 1-Butene. *J. Catal.* **2008**, *254* (2), 180–189.

(26) Song, C.; Chu, Y.; Wang, M.; Shi, H.; Zhao, L.; Guo, X.; Yang, W.; Shen, J.; Xue, N.; Peng, L.; et al. Cooperativity of Adjacent Brønsted Acid Sites in MFI Zeolite Channel Leads to Enhanced Polarization and Cracking of Alkanes. *J. Catal.* **2017**, *349*, 163–174.

(27) Sklenak, S.; Dedecek, J.; Li, C.; Wichterlova, B.; Gabova, V.; Sierka, M.; Sauer, J. Aluminium Siting in the ZSM-5 Framework by Combination of High Resolution 27Al NMR and DFT/MM Calculations. *Phys. Chem. Chem. Phys.* **2009**, *11* (8), 1237–1247.

(28) Yokoi, T.; Mochizuki, H.; Namba, S.; Kondo, J. N.; Tatsumi, T. Control of the Al Distribution in the Framework of ZSM-5 Zeolite and Its Evaluation by Solid-State NMR Technique and Catalytic Properties. *J. Phys. Chem. C* **2015**, *119* (27), 15303–15315.

(29) Zhao, Z.-J.; Kulkarni, A.; Vilella, L.; Norskov, J. K.; Studt, F. Theoretical Insights into the Selective Oxidation of Methane to Methanol in Copper-Exchanged Mordenite. *ACS Catal.* **2016**, *6*, 3760–3766.

(30) McCusker, C. B. and L. B. Database of Zeolite Structures: http://www.iza-structure.org/databases/.

(31) Van Santen, R. A.; Zhidomirov, G. M.; Shubin, A. A.; Yakovlev, A. L.; Barbosa, L. A. M. M. Reactivity Theory of Zinc Cation Species in Zeolites. In *Catalysis by Unique Metal Ion Structures in Solid Matrices: From Science to Application*; Centi, G., Wichterlová, B., Bell, A. T., Eds.; Springer Netherlands: Dordrecht, 2001; pp 187–204.

(32) Shubin, A. A.; Zhidomirov, G. M.; Yakovlev, A. L.; van Santen, R. A. Comparative Quantum Chemical Study of Stabilization Energies of Zn^{2+} Ions in Different Zeolite Structures. *J. Phys. Chem. B* **2001**, *105* (21), 4928–4935.

(33) Lowenstein, W. The Distribution of Aluminium in the Tetrahedra of Silicates and Aluminates. *Am. Mineral.* **1954**, *39*, 92–96.

(34) Dědeček, J.; Sobalík, Z.; Wichterlová, B. Siting and Distribution of Framework Aluminium Atoms in Silicon-Rich Zeolites and Impact on Catalysis. *Catal. Rev.* **2012**, *54* (2), 135–223.

(35) Dunning, T. H.; Hay, P. J. *Gaussian Basis Sets for Molecular Calculations. In Methods of Electronic Structure Theory*; Springer: Boston, MA, 1977.

(36) W. J. Hehre, R. Ditchfield, and J. A. P. Self—Consistent Molecular Orbital Methods. XII. Further Extensions of Gaussian—Type Basis Sets for Use in Molecular Orbital Studies of Organic Molecules. *J. Chem. Phys* **1972**, *56*, 2257.

(37) Oda, A.; Ohkubo, T.; Yumura, T.; Kobayashi, H.; Kuroda, Y. Room-Temperature Activation of the C–H Bond in Methane over Terminal ZnII–Oxyl Species in an MFI Zeolite: A Combined Spectroscopic and Computational Study of the Reactive Frontier

Molecular Orbitals and Their Origins. *Inorg. Chem.* **2019**, *58* (1), 327–338.
(38) Yan, Z.; Zuo, Z.; Li, Z.; Zhang, J. A Cluster DFT Study of NH_3 and NO Adsorption on the $(MoO_2)^{2+}$/HZSM-5 Surface: Lewis versus Brønsted Acid Sites. *Appl. Surf. Sci.* **2014**, *321*, 339–347.
(39) Montejo-Valencia, B. D.; Curet-Arana, M. C. DFT Study of the Lewis Acidities and Relative Hydrothermal Stabilities of BEC and BEA Zeolites Substituted with Ti, Sn, and Ge. *J. Phys. Chem. C* **2015**, *119* (8), 4148–4157.
(40) Mao, X.; Sun, Y.; Pei, S. A Theoretical Investigation into Thiophenic Derivative Cracking Mechanism over Acidic and Cation-Exchanged Beta Zeolites. *Comput. Theor. Chem.* **2015**, *1074*, 112–124.
(41) Sun, Y.; Zheng, D.; Pei, S.; Fan, D. New Theoretical Insights into the Contributions of Poly(Methylbenzene) and Alkene Cycles to the Methanol to Propene Process in H-FAU Zeolite. *J. Phys. Chem. C* **2017**, *121* (30), 16216–16237.
(42) Sung, C.-Y.; Broadbelt, L. J.; Snurr, R. Q. A DFT Study of Adsorption of Intermediates in the NOx Reduction Pathway over BaNaY Zeolites. *Catal. Today* **2008**, *136* (1), 64–75.
(43) Foster, J. P.; Weinhold, F. Natural Hybrid Orbitals. *J. Am. Chem. Soc.* **1980**, *102* (24), 7211–7218.
(44) Frisch, M. J.; Trucks, G. W.; Schlegel, H. B.; Scuseria, G. E.; Robb, M. A.; Cheeseman, J. R.; Scalmani, G.; Barone, V.; Petersson, G. A.; Nakatsuji, H.; et al. Gaussian 16. Wallingford, CT 2016.
(45) Li, G.; Pidko, E. A.; van Santen, R. A.; Feng, Z.; Li, C.; Hensen, E. J. M. Stability and Reactivity of Active Sites for Direct Benzene Oxidation to Phenol in Fe/ZSM-5: A Comprehensive Periodic DFT Study. *J. Catal.* **2011**, *284* (2), 194–206.
(46) Haaland, A.; Green, J. C.; McGrady, G. S.; Downs, A. J.; Gullo, E.; Lyall, M. J.; Timberlake, J.; Tutukin, A. V.; Volden, H. V.; Østby, K.-A. The Length, Strength and Polarity of Metal–carbon Bonds: Dialkylzinc Compounds Studied by Density Functional Theory Calculations, Gas Electron Diffraction and Photoelectron Spectroscopy. *Dalt. Trans.* **2003**, No. 22, 4356–4366.
(47) Martens, J. A.; Jacobs, P. A. Chapter 14 Introduction to Acid Catalysis with Zeolites in Hydrocarbon Reactions. In *Introduction to Zeolite Science and Practice*; van Bekkum, H., Flanigen, E. M., Jacobs, P. A., Jansen, J. C., Eds.; Elsevier, 2001; Vol. 137, pp 633–671.
(48) Haw, J. F. Zeolite Acid Strength and Reaction Mechanisms in Catalysis. *Phys. Chem. Chem. Phys.* **2002**, *4* (22), 5431–5441.
(49) Martínez, A.; Peris, E. Non-Oxidative Methane Dehydroaromatization on Mo/HZSM-5 Catalysts: Tuning the Acidic and Catalytic Properties through Partial Exchange of Zeolite Protons with Alkali and Alkaline-Earth Cations. *Appl. Catal. A Gen.* **2016**, *515*, 32–44.
(50) Pearson, R. G. Chemical Hardness and Density Functional Theory. *J. Chem. Sci.* **2005**, *117* (5), 369–377.

TOC GRAPHICS